Journal Pre-proofs

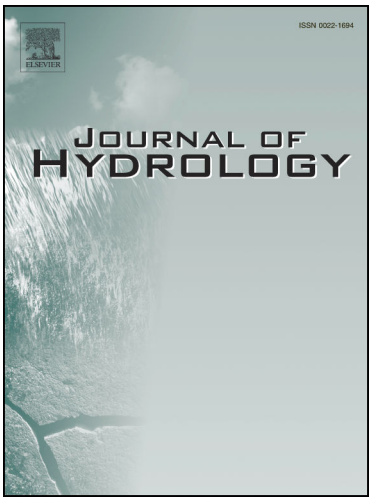


Research papers

# Vertical mixing and horizontal transport unravel phytoplankton blooms in a large riverine reservoir

Bo Gai, Jian Sun, Binliang Lin, Yuanyi Li, Chenxi Mi, Tom Shatwell

PII: S0022-1694(23)01372-0
DOI: https://doi.org/10.1016/j.jhydrol.2023.130430
Reference: HYDROL 130430

To appear in: *Journal of Hydrology*

Received Date: 22 March 2023
Revised Date: 12 October 2023
Accepted Date: 23 October 2023

Please cite this article as: Gai, B., Sun, J., Lin, B., Li, Y., Mi, C., Shatwell, T., Vertical mixing and horizontal transport unravel phytoplankton blooms in a large riverine reservoir, *Journal of Hydrology* (2023), doi: https://doi.org/10.1016/j.jhydrol.2023.130430

# Vertical mixing and horizontal transport unravel phytoplankton blooms in a large riverine reservoir

Bo Gai [a, b], Jian Sun [a], Binliang Lin [a, *], Yuanyi Li [c], Chenxi Mi [b], Tom Shatwell [b]

[a] State Key Laboratory of Hydroscience and Engineering, Department of Hydraulic Engineering, Tsinghua University, Beijing, China

[b] Department of Lake Research, Helmholtz Centre for Environmental Research (UFZ), Magdeburg, Germany

[c] School of Marine Science and Technology, Tianjin University, Tianjin, 300072, China

[*]Corresponding author: Binliang Lin (linbl@mail.tsinghua.edu.cn)

Present address: State Key Laboratory of Hydroscience and Engineering, Department of Hydraulic Engineering, Tsinghua University, Beijing, China

**Abstract:** A precise understanding of the mechanisms causing phytoplankton blooms in reservoirs is still lacking, especially in large riverine reservoirs. To better understand these blooms, the role of the complex hydrodynamics caused by dam operation must be quantified. Here we examine how synergistic hydrodynamic processes, rather than individual metrics, trigger blooms in Xiangxi Bay, a typical tributary bay of the Three Gorges Reservoir, China. We used a 3D ecological-hydrodynamic model, which integrated hydrodynamics with the abiotic factors that limit phytoplankton growth to simulate one whole year (2010). By implementing a scaling criterion, we quantified the contribution of local phytoplankton growth and hydrodynamic processes, including advection transport and vertical mixing, on bloom dynamics. Results indicated vertical mixing was the main process inhibiting blooms in colder months (from October to February) but horizontal advection, which flushed and diluted blooms, was dominant in warmer months (from May to July) when stratification was intense and nutrients were replete. Accordingly, blooms occurred when both vertical mixing and horizontal advection were low. We suggested a potential dam operation strategy to mitigate blooms during stratification, which involves withdrawing the warm surface water from upstream reservoirs to increase horizontal flows in the surface layer. Extending the application of critical turbulence model, our study shows how vertical mixing and horizontal advection rate interact with phytoplankton growth rate to drive blooms in highly dynamic riverine systems.

**Keywords:** Phytoplankton bloom dynamics; Vertical mixing; Advection transport; Three-dimensional ecological-hydrodynamic model; Three Gorges Reservoir; Dam operation.

## 1. Introduction

Phytoplankton blooms threaten lakes and reservoirs globally (Paerl et al., 2011), and their occurrence and severity are anticipated to increase as a result of continuous human-driven nutrient loading and climate change (Paerl and Huisman 2010, Visser et al., 2016, Janssen et al., 2019). Many studies have investigated the variables that influence phytoplankton blooms in lakes, mostly concentrating on nutrient loading, lake-specific geomorphological and ecosystem properties including lake depth, size, light climate, and water temperature (Scheffer and Van 2007, Paerl and Huisman 2008, Hai et al., 2010). Phytoplankton growth is affected by light, water temperature, and the supply of nutrients, but bloom formation also depends on hydrodynamics and loss processes like grazing and sinking. As artificial structures, reservoirs possess different morphological characteristics from natural lakes. They are often long and narrow, featuring a major inflow, with possibly several tributaries, and an outflow at or near the dam (Zhang et al., 2020). Impounded rivers have both lacustrine and riverine characteristics to varying degrees, where more riverine systems possess significant horizontal flows. In all cases, dams can change the discharge characteristics, lower the flow velocity, prolong the retention time, and often cause stratification (Marshall and Burchardt 1998, Mcgregor and Fabbro 2000, Mitrovic et al., 2010). These factors increase the likelihood of phytoplankton blooms. However the mechanisms by which hydrodynamic conditions affect bloom dynamics are complex (Sha et al., 2015, Song et al., 2021, Huang et al., 2022), especially in large riverine reservoirs, and warrant further investigation (Song 2023).

As one of the largest hydropower projects in the world, the Three Gorges Reservoir (TGR) was constructed to effectively control floods in the Yangtze River, provide abundant electric power, and improve shipping. The TGR is a typical riverine reservoir in which the hydrodynamic processes play a vital role in the physical, biogeochemical and ecological characteristics. Since the reservoir impoundment, the water level has risen significantly, the flow velocity in the reservoir has greatly slowed, the water exchange has weakened, and the self-purification capacity of the waterbody has decreased (Liu et al., 2013). As a result, many tributary bays of the TGR have suffered phytoplankton blooms of different scales each year, especially in 2008 when Xiangxi Bay (XXB), a typical tributary bay of the TGR, suffered severe cyanobacteria blooms (Ministry of Environmental Protection of China 2014). The water flow in the XXB is not obstructed by a dam, but is heavily disrupted by the main reservoir (Dai et al., 2013). Due to complex bidirectional currents rather than direct flow from upstream to downstream (Andreas et al., 2014), the hydrodynamics in certain tributary bays of the TGR differ from those observed in most other reservoirs across the world (Yang et al., 2018b). Most studies in this type of reservoir have focused on how single hydrodynamic aspects affect phytoplankton blooms, such as flow velocity, retention time, density currents, water level fluctuation, thermal stratification, circulation, and fluctuations in light supply due to vertical mixing (Ji et al., 2017, Köhler et al., 2018, Li et al., 2021, Ishikawa et al., 2022). However, hydrodynamics are complex, and a single parameter cannot represent all processes. To address this, Yang et al., (2022) included three hydrodynamic parameters (flow velocity, water retention time, and stratified structure), to identify the most sensitive parameter affecting algae growth via a series of experiments. These aspects were studied independently, however, hydrodynamic effects can be synergistic. For instance, stratification, long water residence times and low flow velocities collectively promote phytoplankton blooms (Song 2023). These individual or independent

parameters cannot adequately represent synergistic hydrodynamic processes and therefore, additional research is required to understand how coupled hydrodynamics and environmental conditions interact to drive phytoplankton blooms in this type of tributary bay.

In tributary bays like the XXB, the flow characteristics are strongly three-dimensional, such as the water exchange in the intersection area between the main stream and tributary, the circulation and the internal waves in the bay, which cannot be properly mimicked in a one-dimensional or two-dimensional approach (Bocaniov et al., 2014). However, due to the high computational effort, many three-dimensional ecological modelling studies on phytoplankton in freshwater systems mainly concentrated only on short-term phytoplankton blooms (Hedger et al., 2004, Amour and Kauranne 2017, Li et al., 2018), and insights into the seasonal variations of phytoplankton blooms and their influencing factors are therefore limited. Also, since phytoplankton production varies with all the physical processes in the model, their findings are sometimes challenging to interpret. It is necessary to differentiate and quantify the role of hydrodynamic processes in bloom dynamics through long-term numerical simulations.

To fill these knowledge gaps, a three-dimensional ecological-hydrodynamic model was established to simulate one whole year (2010) in the XXB. The seasonally varying role of hydrodynamics, like advective transport and vertical mixing, as well as environmental factors like temperature, light and nutrients, to the development of phytoplankton blooms, were attributed. For this, a scaling criterion (Liu and de Swart 2015, Liu et al., 2018) was applied, which formulated the equation governing phytoplankton dynamics, and unified the non-local hydrodynamic processes and local growth of phytoplankton on a comparable scale with the same unit. We implemented this approach into our 3D numerical model, for the first time, to quantify and compare net growth and hydrodynamic effects in the productive zone. The main targets of this study are to 1) quantify the role of advection and diffusion processes on bloom dynamics; 2) determine the drivers of phytoplankton blooms and seasonal patterns; 3) propose potential ways of mitigating blooms in tributary bays of the TGR and perspectives for future research. The findings contribute to a better understanding of the mechanism of phytoplankton blooms in tributary bays of large riverine reservoirs and provide a new insight for estimating hydrodynamic influence on phytoplankton dynamics.

## 2. Material and methods

### 2.1. Study site

The TGR is one of the largest artificial reservoirs in the world (Fig. 1a). This riverine reservoir is very long (667 km) when the water level reaches 175 m above sea level at the end of autumn and winter. It has a total surface area of about 1084 $km^2$ and total storage capacity of $39.3 \times 10^9$ $m^3$. The TGR is located in a subtropical climate, with an average air temperature of 17.6 °C and an average monthly water temperature above 10 °C. The TGR operation cycle is divided into four stages according to water level and discharge: normal operation (November to January), drawdown (February to early June), low water level operation (June to August) and impoundment (September to October) (Li et al., 2020). Xiangxi River, which is one of the TGR's largest tributaries, flows into

the reservoir 32 km upstream of the Three Gorges Dam. The main stream of the Xiangxi River is about 94 km long, the basin area is 3099 $km^2$, the average annual flow is 47.3 $m^3 s^{-1}$, and the maximum discharge can reach 300 $m^3 s^{-1}$. The average monthly retention time in XXB ranges from 7 to 16 days (Liu et al., 2013). Before the impoundment of the TGR in 2003, the flow velocity in the Xiangxi River was very fast due to its large bed slope (2.7‰), and no phytoplankton blooms were reported. The impoundment of the TGR significantly increased the water level, greatly reduced the velocity in the Xiangxi River, and formed a bay called Xiangxi Bay. Seasonal stratification, especially strong summer stratification, occurred in XXB, whereas the mainstream of the TGR is seldom affected by seasonal stratification due to the large runoff and strong mixing (Long et al., 2022).

The research area (Fig. 1b) includes 32 km of the river reach of the Xiangxi River from the upper reaches of Zhaojun Town to the intersection of the Xiangxi and Yangtze Rivers, and a 7 km reach of the Yangtze River at the intersection to the XXB. Water temperature, flow velocity, and water quality indicators are measured at observation points A01, A04, A07, A10, and XX06 in the XXB. Profiles of water temperature and velocity were measured with a Hydrolab DS 5X multi-probe sonde (Hach, USA) and an Acoustic Doppler Vector velocimeter (ADV; Nortek, Norway). Surface water samples were collected and transported to the laboratory for water quality indicator analysis (chlorophyll a (chl-a), nitrate, ammonia, and phosphate) using the national standard method (Liu et al., 2012, Xu et al., 2021). Water temperature and flow velocity profiles and time-series of surface water quality indicators were used for model validation.

### 2.2. Model description and setup

1) Hydrodynamic model

The TGR impoundment increased the water surface width in the lower reach of the XXB to 300 - 600 m. Nevertheless, compared to the horizontal direction, the vertical water flow is comparatively weak. For such a condition, the shallow water equations with the Boussinesq approximation are appropriate for characterizing the water movement in the XXB. In this study, the three-dimensional model Delft3D-Flow (developed by Deltares, a research institution based in Netherlands) was applied to simulate the hydrodynamics in the XXB. An orthogonal curvilinear grid is used in the horizontal direction and z-coordinate, or σ-coordinate is used in the vertical direction. Considering the steep topography of the XXB in our study, the z-coordinate system was selected to better calculate the vertical exchange processes due to the existence of vertical stratification. The model solves shallow water equations (with the hydrostatic and Boussinesq hypotheses) derived from the Reynolds-averaged Navier-Stokes equations for an incompressible fluid, and the k-ε turbulence model is utilized to determine the vertical eddy diffusion caused by turbulent mixing. The Delft3D-Flow model can effectively solve the shallow water equations in the horizontal direction by using the Alternative Direction Implicitly (ADI) approach (2D). The vertical velocity is calculated by integrating the mass conservation equations and the horizontal velocities averaged over the water depth. More details are given in Deltares (2013).

2) Water quality model

The water quality module, Delft3D-WAQ, driven by the hydrodynamic model, was applied to the XXB to simulate water quality and ecological conditions. It offers a framework for a variety of substances and processes selected by the user, giving the model tremendous versatility. For the present study, phytoplankton, nutrients and dissolved oxygen dynamics were investigated, including phytoplankton utilization of inorganic nutrients, production of oxygen through photosynthesis, consumption of dissolved oxygen, and release of organic matter through respiration. Organic carbon, organic nitrogen, and organic phosphorus are transformed into inorganic forms via mineralization and hydrolysis, and undergo a variety of reactions in the model that consume dissolved oxygen. More details of the biogeochemical processes can be found in the relevant references in Deltares (2013). The central principle of the water quality simulation is to solve the advection-diffusion-reaction equation, namely, the mass balance equation. The mass balance equation for phytoplankton may be generally expressed as:

$$\frac{\partial C}{\partial t} = \underbrace{-\frac{\partial uC}{\partial x} - \frac{\partial vC}{\partial y} - \frac{\partial wC}{\partial z}}_{\text{Advective transport}} + \underbrace{\frac{\partial}{\partial x}\left(D_h \frac{\partial C}{\partial x}\right) + \frac{\partial}{\partial y}\left(D_h \frac{\partial C}{\partial y}\right) + \frac{\partial}{\partial z}\left(D_v \frac{\partial C}{\partial z}\right)}_{\text{Dispersive transport}} + \underbrace{\left(\frac{\partial S}{\partial z} + P - R - M\right)C}_{\text{Biogeochemical variation}} \quad (1)$$

where $C$ is the concentration of phytoplankton (mg C $m^{-3}$); $D_h$ and $D_v$ are turbulent diffusivities in the horizontal and vertical directions ($m^2$ $s^{-1}$), respectively; $u$, $v$ are the horizontal velocity components (m $s^{-1}$), and $w$ is the vertical velocity components (m $s^{-1}$). The source and sink terms for phytoplankton include growth, respiration, mortality and settling. $P$ is the gross phytoplankton growth rate ($day^{-1}$); $R$ is the phytoplankton respiration rate ($day^{-1}$); $M$ is the phytoplankton morality rate ($day^{-1}$) and $S$ is the phytoplankton settling velocity (m $day^{-1}$). Note that the general mass balance equation Eq. (1) is also used for all chemical and biological variables in the water column such as nutrients and dissolved oxygen. The only difference is that different variables have different process formulations for the 'source and sink' terms.

Phytoplankton growth is assumed to be mainly dependent on water temperature, light and nutrients, which can be expressed as:

$$P = P_{\max} \times f_1(L) \times f_2(C_N) \times f_3(T) \quad (2)$$

where $P_{\max}$ is the maximum phytoplankton growth rate at a reference temperature of 20 °C ($day^{-1}$); $f_1(L)$ is the light limitation factor (-); $f_2(C_N)$ is the nutrient limitation factor (-); and $f_3(T)$ is the water temperature limitation factor (-). The details of the limiting factor calculations are provided in Text S1 in the SI.

### 2.3. Model configuration and calibration

We adopted a hydrodynamic model for the XXB established in a previous study using the Delft3D-Flow module. This hydrodynamic model was effectively validated against the observational

velocity and water temperature data (Li et al., 2020). The model has two upstream boundaries and one downstream boundary (Fig. 1b). The XXB upstream boundary is located close to Zhaojun Town, and the upstream boundary of the Yangtze River is located near Guizhou Town. The downstream boundary of the Yangtze River is set 4 km downstream from the intersection area of the XXB. Based on the hydrodynamic model, we further developed an ecological-hydrodynamic model for the XXB by incorporating the Delft3D-WAQ biogeochemical module. Inflow nutrient concentrations (nitrate, ammonia, orthophosphate) were obtained from monthly sampling data and were set as the upstream boundary conditions for XXB and the Yangtze River. The nutrient concentrations at the Yangtze River downstream boundary were set the same as at the Yangtze River upstream boundary, as the nutrients were uniformly distributed in the section of the Yangtze River we calculated, and the spatio-temporal distribution of biogeochemical processes in the XXB was not sensitive to the condition of nutrients at the downstream boundary of the Yangtze River. The phytoplankton concentration was set to zero at all the boundaries due to the very low chl-a values in the XXB upstream inflow and the Yangtze River. The model simulation ran from June 01, 2009 to December 31, 2010, with a cold start (the velocity was set to zero, the phytoplankton concentration was set to 0.01 mg $m^{-3}$, the temperature and nutrients were set to the arithmetic mean of values of the boundaries). The half-year simulation in 2009 was for spin-up to make the model stable and the results reliable, and the 2010 results were used for analysis. The time step was set to 0.6 min.

In addition to the validation by (Li et al., 2020), we further validated the hydrodynamic model with an additional six vertical water temperature profiles and five velocity profiles at different stations and dates, in order to establish a good foundation for the water quality simulation (Fig. S1 and S2). For water quality calibration, as many parameters as possible should be determined *a priori* by ecological background knowledge and empirical evidence in order to incorporate ecological understanding of the important processes. This produces a more robust, transferable model. Therefore, we determined the parameters based on the related literature (Bowie et al., 1985, Carraro et al., 2012, Lian et al., 2014, Mao et al., 2015, Chuo et al., 2019), especially modelling studies at the same study site, ecological background knowledge, and evaluation of field experiments in the TGR. We were then able to determine all parameters of the ecological model *a priori* except the two key parameters: the temperature constant for production and light saturation coefficient, which were calibrated manually by 'trial and error' (Carraro et al., 2012, Robson et al., 2013, Song et al., 2022), to minimize the error (inferred by *RMSE*) for chl-a concentration and yield good spatio-temporal distribution of phytoplankton blooms according to in situ observations (Liu et al., 2012, Yang et al., 2018b). Statistical indices, such as the mean absolute error (*MAE*) and the *RMSE* were used to quantitatively assess the quality of fit and errors between the observed and simulated data. The formulations are presented as follow:

$$MAE=\frac{\sum_{i=1}^{n}\left|X_{obs,i}-X_{model,i}\right|}{n} \qquad (3)$$

$$RMSE=\sqrt{\frac{\sum_{i=1}^{n}\left(X_{obs,i}-X_{model,i}\right)^{2}}{n}} \qquad (4)$$

Our model was carefully calibrated and validated against measurement data (see Text S2 in SI) and showed good performance in light of water temperature (Fig. S1), velocity (Fig. S2), and water quality indicators (Fig. S3). The water quality parameters used in this study are shown in Table 1.

### 2.4. Scaling of physical and growth processes and data handling

To gain insight into the mechanisms that underlie the phytoplankton bloom dynamics, the contributions of advection and diffusion terms that influence the phytoplankton growth were quantified. This was done by rewriting Eq. (1) as

$\mu$: local (net specific growth) process rate

$$\frac{1}{C}\frac{\partial C}{\partial t} = \left(\frac{\partial}{\partial z} + P - R - M\right) \qquad \text{Advection loss} \quad \text{Diffusion loss}$$

$$-\frac{1}{C}\left[\frac{\partial uC}{\partial x} + \frac{\partial vC}{\partial y} + \frac{\partial wC}{\partial z} - \left[\frac{\partial}{\partial x}\left(D_h \frac{\partial C}{\partial x}\right) + \frac{\partial}{\partial y}\left(D_h \frac{\partial C}{\partial y}\right)\right] - \frac{\partial}{\partial z}\left(D_v \frac{\partial C}{\partial z}\right)\right] \qquad (5)$$

$\Psi$: non-local (hydrodynamic) loss rate

The left-hand side indicates the overall growth rate of $C$ at a fixed position. We divided the right-hand side into two terms: $\mu$ related to local (specific net growth of phytoplankton) processes and $\Psi$ related to non-local (hydrodynamic) processes. $\Psi$ in turn consists of advection and diffusion components. All terms have units of day$^{-1}$. The term "advection loss" has two constituents related to horizontal and vertical advection, and the term "diffusion loss" has two constituents related to horizontal and vertical diffusion. In view of the research objective and hydrodynamic condition in XXB, horizontal advection and vertical mixing are the dominant terms that lead to the negative contribution to the gross phytoplankton growth rate (Liu et al., 2018). Accordingly, we extracted the horizontal advection and vertical diffusion terms from the three-dimensional modelling results as follows:

Horizontal advection loss $$\frac{1}{C}\left(\frac{\partial uC}{\partial x} + \frac{\partial vC}{\partial y}\right) = \frac{\partial u}{\partial x} + \frac{\partial v}{\partial y} + \frac{1}{C}\left(u\frac{\partial C}{\partial x} + v\frac{\partial C}{\partial y}\right) \sim \frac{1}{C}\left(u\frac{\partial C}{\partial x} + v\frac{\partial C}{\partial y}\right) \qquad (6)$$

Vertical diffusion loss $$\frac{1}{C}\left[-\frac{\partial}{\partial z}\left(D_v \frac{\partial C}{\partial z}\right)\right] \qquad (7)$$

In Eq. (6), the first two terms on the right hand side $\frac{\partial u}{\partial x}$ and $\frac{\partial v}{\partial y}$ are only of the order of $10^{-2}$-$10^{-3}$ d$^{-1}$ in our study, which is ~two orders of magnitude smaller than the last two terms on the right hand side. Also, $\frac{\partial u}{\partial x}$ and $\frac{\partial v}{\partial y}$ are usually ignored in many water quality modelling studies, e.g., Huisman et al.,

(1999), Marcé et al., (2007), Liu et al., (2018). Thus, we took the last two terms of the equation to analyse advection loss. All of these hydrodynamic terms, like the advection loss, diffusion loss, and the non-local loss rate, were accessed via modifying the source code of Delft3D. This makes it possible to output the integrated hydrodynamic processes rather than the single hydrodynamic variables.

We also analysed the mixed layer depth (MLD), which was inferred as the depth at which the temperature was 0.5 °C lower than that at the surface (de Boyer Montégut 2004) according to several other studies at the same study site (Xu et al., 2021, Yang et al., 2022). Moreover, this method was shown to be particularly insensitive to vertical resolution of water temperature data, while the temporal pattern was relatively robust to changes in the threshold value (Wilson et al., 2020), especially considering the complex hydrodynamics in the XXB. Phytoplankton blooms were inferred when Chl-a concentration exceeded 30 mg $m^{-3}$ (Yang et al. 2022) and bloom impact area was defined where Chl-a concentration exceeded 30 mg $m^{-3}$. Winter was defined as December to the following February, spring as March to May, summer as June to September, and autumn as October to November.

## 3. Results

### 3.1. Thermal stratification, mixed layer depth and circulation patterns

In XXB (Fig. 2a-c), the water temperature varied from 11 °C to 30 °C throughout the year, with the lowest water temperature in March and the highest in August. In winter, the temperature difference between the surface and bottom layers was small, only about 0.5 °C, and there was no stratification. In spring, thermal stratification was enhanced and the temperature difference between the surface and bottom reached ~4 °C. In summer, the temperature difference increased to ~8 °C, forming strong thermal stratification at the surface layer. From the end of June to the beginning of August, a very thin layer of warm water (dashed box in Fig. 2) appeared on the surface in the middle and upper reaches. The temperature gradient was large, reaching ~1.5 °C $m^{-1}$, which might be the consequence of high air temperature during this period. During the subsequent TGR impoundment in autumn, the water level rose rapidly and the main stream water intruded into the XXB. The waterbody was mixed and the thermal stratification disappeared gradually.

In spring and summer, the thermocline normally appeared in a very shallow water layer, and the MLD was small (less than 10 m in most cases). From the end of June to the beginning of August, the MLD was even less than 5 m due to the strong stratification on the surface layer. In autumn and winter, the thermocline appeared at the bottom, and the MLD was large (about 40 m).

At the intersection area (Fig. 2d), water temperature ranged from 11 °C to 28 °C and there was no obvious thermal stratification throughout the year with surface-bottom temperature differences ranging between 0.2 °C and 2 °C.

Due to the density distinction produced by temperature difference between the main stream and tributary, the density currents from the main stream intruded into the XXB from the surface, middle, and bottom layers at various times. For instance, during the low water level operation (June to

August), currents occasionally intruded into the middle layer and generated complex circulation patterns (Fig. 4a and b). At the beginning of this period, the main stream water intruded into the XXB from the middle layer of the intersection and flowed 25 km upstream before it plunged and flowed back to the main stream along the river bed (Fig. 4a). At the end of this period, the main stream water intruded into the XXB again from the middle layers, but instead of plunging, the intruding water flowed back towards the main stream along the surface. During the whole period, the upstream inflow was colder than the water in the bay, and the upstream density currents always plunged and flowed along the river bed to the main stream (Fig. 4b).

### 3.2. Seasonal and spatial distribution of phytoplankton bloom

Phytoplankton blooms in the simulation mainly occurred in the middle and upper reaches (Fig. 3a and b). There were four extended blooms (marked by dashed lines) between mid-March and mid-September, with the longest bloom (50-100 mg $m^{-3}$ Chl-a) from June to August. The maximum value (120 mg $m^{-3}$) occurred in mid-April at the middle reach (shown by the black arrow in Fig. 3b). Blooms generally developed in the upper 15 m of the bay due to the vertical light attenuation. In summer, the maximum water depth at which a bloom could develop was only ~5 m because of the self-shading effect. In the lower reaches (Fig. 3c), large-scale phytoplankton blooms only occurred once in August, with the Chl-a concentration exceeding 100 mg $m^{-3}$, and lasted for nearly one month. Phytoplankton blooms in other periods were smaller and shorter in duration. At the intersection (Fig. 3d), the Chl-a concentration did not exceed 30 mg $m^{-3}$ over the whole year due to the strong mixing.

The spatial distributions of the spring and summer blooms differed significantly. The spring phytoplankton blooms (Fig. 3e) occurred in the middle and upper reaches, mainly concentrated in the depth above ~15 m. The Chl-a concentration in the middle reaches was higher than the upper reaches. The impact area was relatively small (~7 km) while the overall Chl-a concentration was high. The summer phytoplankton blooms (Fig. 3f) occurred in all upper, middle, and lower reaches, mainly concentrated in the top 5 m water layer. The impact area extended to the entire bay (over 20 km), with a lower overall Chl-a concentration compared to spring blooms.

### 3.3. Interaction between circulation patterns and phytoplankton blooms

The Chl-a concentration distribution and circulation patterns during the collapse of a phytoplankton bloom in a week at the end of July are shown in Fig. 4. At the beginning of this period, the circulation exhibited a clockwise pattern, and the surface currents flowed from the main stream to the upstream (Fig. 4a). At the end of this period, main stream the circulation pattern altered from the clockwise to anti-clockwise, and the surface currents flowed downstream to the main stream (Fig. 4b). The phytoplankton in the surface layer in the upper-middle reaches merged with the main stream due to the shift in the circulation patterns, and then the phytoplankton blooms disappeared gradually.

In terms of the horizontal Chl-a distribution, at the beginning of this period, the Chl-a concentration near A07 was very high (~80 mg $m^{-3}$), and the phytoplankton bloom impact area was

~10 km in a range from 20 to 30 km away from the intersection (Fig. 4c). As the circulation pattern altered, the high Chl-a area was brought to the main stream by the surface currents. The Chl-a concentration was gradually diluted, and the phytoplankton bloom collapsed (Fig. 4d). However, the impact area was extended to the entire bay.

### 3.4. Impacts of non-local processes and local growth on phytoplankton blooms

The Chl-a concentration variation had a clear negative correlation with the MLD (Fig. 5a). In autumn and winter, the MLD was large (~40 m) and Chl-a concentration was low (less than 5 mg $m^{-3}$). The deeper mixing leads to lower average light in the mixed layer, which is not sufficient to cause a bloom. In spring and summer, the MLD was very small (mostly 5-10 m), with the smallest value in summer (less than 5 m). The phytoplankton were maintained in this very thin surface layer and two long-term phytoplankton blooms occurred: the spring bloom from Mid-March to May and the summer bloom from July to September. There were several short-term blooms, twice in May and once in September.

The non-local (hydrodynamic) loss rate $\psi$ to phytoplankton accumulation was large in autumn and winter, especially from October to December, the maximum $\psi$ value reached 4 $day^{-1}$ (Fig. 5b). In spring and summer, $\psi$ also reached very large values from April to June. When $\psi$ was lower than the local (specific net growth of phytoplankton) process rate $\mu$, the Chl-a concentration increased sharply and phytoplankton blooms occurred (shown in yellow shades). On the other hand, when $\psi$ was greater than $\mu$, Chl-a concentration decreased rapidly. Even during the phytoplankton bloom period in July-August, a transient peak in $\psi$ (orange arrow in Fig. 5) caused a strong drop in Chl-a concentration (green arrow), whereas the Chl-a recovered quickly when $\psi$ decreased again. The relative relationship between $\psi$ and $\mu$ was the main factor driving the growth and collapse of phytoplankton blooms. In addition, in colder months (from October to February) vertical diffusion was the leading term that results in the negative contribution to the total growth rate, while the horizontal advection process dominated in warmer months (from May to July) when the vertical diffusion process was very weak (Fig. 5c).

We calculated the limitation of environmental factors on *P* in the surface layer (the surface layer of our model, with a depth of 1.5m). The limitation factor of nitrogen was between 0.9 and 1.0 throughout the year, where a value of 0 indicates complete limitation, and 1 indicates no limitation. The limitation factor of phosphorus was even higher than 0.95 (Fig. 6a and b). This indicated that nutrients were replete and had almost no limiting effect on the specific phytoplankton growth *P*. As shown in Fig. 6c, the limitation of light energy in the surface layer was relatively low from July to September, and the median value was between 0.75-0.85, which might be caused by self-shading. Except for this period, the limitation factor of light fluctuated slightly, and the median value was between 0.9 and 1.0. Light is a complex resource, and growth can be constrained not only by suboptimal light energy, but also because its temporal pattern is suboptimal (Nicklisch et al., 2008). The model accounts for this with the daylength factor (Fig 6e). Daylength further constrained the growth rates seasonally, with the strongest limitation in winter with values around 0.5. It was highest in June – August, with values ranging between 0.75 and 0.95.Temperature also constrained *P* with a certain seasonal trend (Fig. 6d). The water temperature was lowest in March and April (~11 °C), and the temperature limitation factor was ~0.85. The water temperature was high from June to October

(23-30 °C) when the temperature limitation factor was greater than 1.0.

## 4. Discussion

### 4.1. Mechanisms underlying phytoplankton bloom dynamics

The calibrated and validated 3D model could well reproduce the spatial and seasonal distribution of thermal stratification and phytoplankton blooms. The simulated seasonal trends of the MLD and Chl-a concentration as well as the onset and break-up of phytoplankton blooms were consistent with the results of previous observation studies in the XXB (Liu et al., 2012, Yang et al., 2018b). Thus, our model provided a solid basis for analysing the driving factors affecting phytoplankton blooms.

Many existing studies discussed nutrients and water temperature as the drivers of phytoplankton blooms (Paerl and Huisman 2008, Huisman et al., 2018). In the current study, we found the limitation of nutrients to the local (specific net growth of phytoplankton) process rate $\mu$ was low throughout the year, indicating that the nutrients in the XXB were sufficient (Fig. 6a and b). The temperature limitation was strongest in March and April, yet a large-scale spring bloom still occurred. Clearly ample nutrients and sufficiently high temperature are prerequisites for the blooms, but they did not explain their dynamics, nor what triggered them.

Blooms form and collapse according to the balance between growth and losses. Eq. (5) shows that nutrients, light and temperature only affect $\mu$. However, the non-local (hydrodynamic) loss rate $\psi$ also plays a vital role in the accumulation and dissipation of blooms. In the current study, the maximum specific growth rate $P_{max}$ was set to 1.8 $\mathrm{day}^{-1}$ (black dashed line in Fig. 5b). When the absolute value of $\psi$ exceeded this value, no phytoplankton bloom could form, regardless of any environmental limitation.

Thermal stratification contributes to phytoplankton blooms in spring (Sommer et al., 1986, Nicklisch et al., 2008) and summer (Jöhnk et al., 2008). Thermal stratification restricts the vertical turbulence, hence the majority of phytoplankton can stabilize in the water near the surface with sufficient light, eventually leading to a phytoplankton bloom. This effect is enhanced by higher growth rates due to a more steady light supply in shallow mixed layers (Shatwell et al., 2012, Köhler et al., 2018). According to research conducted on 40 reservoirs, thermal stratification was the primary driver of phytoplankton in reservoirs (Mcgregor and Fabbro 2000). The TGR field monitoring revealed that phytoplankton blooms always occurred in the spring and collapsed in the autumn, which was in good agreement with the decrease and increase of the MLD (Yang et al., 2013). We found that the seasonal trends of Chl-a concentration negatively correlated with the MLD, which indicated that the growth and collapse of phytoplankton blooms in the XXB was closely related to the changes in the mixing states in the surface layer (Fig. 5a). Although this is consistent with the critical depth hypothesis (Sverdrup 1953), which states that average light is too low in deep mixed layers to support net growth and was applied to explain bloom dynamics in XXB (Liu et al., 2012, Yang et al., 2022), our results suggested this finding is more in line with the critical turbulence hypothesis (Huisman et al., 1999), which states that blooms can form when phytoplankton can grow faster than they are transported downwards by turbulence. Our analysis clearly showed that the

vertical turbulent diffusive transport exceeded the net growth rates in the surface bloom layer during periods when the mixed layer was deep before March or after September (Fig. 5c), preventing a bloom. On the other hand, when the diffusive transport fell below the net growth rate in March, a large bloom began. Our use of the non-local diffusion rates as a metric with the same scale as the local growth rate ($d^{-1}$) can better explain the interaction between mixing processes and local processes than the MLD (Xu et al., 2021, Yang et al., 2022). Additionally, this better illustrated how the critical turbulence hypothesis unravelled bloom dynamics in autumn and winter.

However, one unanticipated finding was that the Chl-a concentration also dropped significantly during periods when the MLD was low (i.e. from April to June shown in blue shades in Fig. 6). During this period of intense stratification, light, water temperature and nutrients were sufficient to support fast growth, which exceeded the vertical turbulent transport losses (close to 0 due to the intense stratification), but there was still no phytoplankton bloom. Clearly, we can get an explanation from Fig. 5c. Here, the longitudinal advection was the dominant term that resulted in the negative contribution to the total growth rate. Due to the influence of the density intruding currents from the main stream and the upstream inflow, the surface flow velocity increased, and the circulation pattern shifted. The advective effect played a decisive role in the collapse of blooms during this period. These results demonstrate a key finding in dynamic riverine lakes and reservoirs that goes beyond the critical turbulence hypothesis: not only the vertical diffusion, but also the horizontal advection determine bloom formation. Previous studies have already stated the vital influence of advection on algal biomass accumulation in advection-dominated waterbodies (Soballe and Kimmel 1987, Reynolds 2000, Burford et al., 2007, Lucas et al., 2009). However, most of these studies applied bulk metrics, e.g., residence time, which do not indicate the spatio-temporal distribution of horizontal advection. By employing the scaling approach, our study differentiated and quantified vertical mixing and horizontal advection in the same scale as local algae growth to explicitly unravel how vertical mixing and horizontal transport spatially and temporally interact to drive blooms. Bulk metrics like residence time and MLD are less likely to capture these integrated hydrodynamics at the resolution necessary to understand bloom dynamics. Additionally, our analysis method is well suited to and, could be incorporated into the critical turbulence concept by including the dilution of phytoplankton by flushing in reservoirs with strong riverine characteristics.

Prior studies have noted the importance of circulation in terms of carrying large amounts of nutrients into the tributaries, which provides sufficient nutrients for phytoplankton growth (Zhang et al., 2012, Yang et al., 2018a). However, our study emphasized the direct effects of advective processes on phytoplankton, such as flushing and dilution, which played a more significant role in the appearance and disappearance of phytoplankton blooms. In lakes and reservoirs with weak hydrodynamics, it is feasible to ignore the advection term when simulating and analyzing blooms. However, in rivers, and in riverine reservoirs with intense hydrodynamic conditions, the effect of advection on growth and collapse of phytoplankton blooms should not be ignored.

### 4.2. Implications and perspectives

Many previous studies stated that stratification was the dominant driver for phytoplankton

blooms in XXB (Liu et al., 2012, Chuo et al., 2019, Xu et al., 2021, Yang et al., 2022), whereas some other studies focused on the horizontal processes, e.g., intruding currents and circulations (Long et al., 2019, Li et al., 2021), water exchange and transport (Gao et al., 2018, He et al., 2023). Our study revealed, for the first time, that blooms were inhibited alternatively by vertical mixing and horizontal transport processes in colder and warmer months, respectively. This will also provide new insights into potential strategies to mitigate blooms.

Phytoplankton blooms in tributary bays of the TGR can likely be suppressed by reducing nutrient loads, and it is believed a feasible approach in many other lakes and reservoirs (Schindler et al., 2016, Wurtsbaugh et al., 2019). However, many scholars noted that nutrients in these tributary bays were more affected by the main stream of the Yangtze River (Holbach et al., 2014, Xiang et al., 2021), which originate mainly from the entire upstream basin of the Yangtze River. Due to the vast upstream catchment of the TGR, nutrient load reduction is unlikely to be successful in the short term without significant influence on local agriculture, industry and life (Fu et al., 2010, Yang et al., 2015). Therefore, efforts to improve the water quality in those bays through pollution control will instead be a long-term task. Currently, most studies have concentrated on breaking the thermal stratification to reduce phytoplankton blooms (Visser et al., 2015, Dutta and Das 2020). Dam operations like enlarging the daily water level fluctuations, and increasing duration of water level rise, etc., were explored and demonstrated to be an effective method to control phytoplankton blooms in tributary bays of the TGR by disrupting water stratification (Zhou 2006, Sha et al., 2015, Gao et al., 2018). However, since the TGR is mainly used for flooding control and electricity generation, such dam operation will obviously affect reservoir security as well as economic benefits.

In advection dominated periods, altering the circulation patterns is potentially also an alternative. When the simulated phytoplankton blooms occurred frequently in spring and summer (yellow shades in Fig. 5), the intruding water mainly entered the bay from the surface layer, or the middle layer, and flowed back to the main stream along the river bed (Long et al., 2019, Li et al., 2020). The circulation pattern was vertically clockwise as shown in Fig. 4a: surface currents flowed upstream before plunging and flowing back downstream. This was not conducive to the collapse of phytoplankton blooms because it did not destabilize the water column or significantly increase $\psi$ as discussed in 4.1. In autumn and winter, the main stream water mainly intruded into the bay in the deeper parts of the water column. From there it traced upstream along the river bed, and then flowed back to the main stream from the surface layer. The circulation pattern during this period is mainly anticlockwise as shown in Fig. 4b: the surface current flowed downstream, which helped to suppress and dilute phytoplankton blooms due to a high hydrodynamics loss rate.

In the upstream of the tributaries of the TGR, there are many cascade reservoirs. A selective withdrawal strategy could be adopted (Mi et al., 2022, Mi et al., 2023, Song et al., 2023), for example, withdrawing the surface warm water from upstream cascade reservoirs, which could shift the circulation patterns in the tributary bays so that the upstream inflow flows downstream from the surface layer and forms an anti-clockwise circulation. This may be a potential way to control the phytoplankton blooms. Nevertheless, the actual effects of the selective withdrawal strategy on preventing phytoplankton blooms need to be studied in more detail using withdrawal model scenarios, and this could be a perspective for future research.

## 5. Conclusions

Phytoplankton dynamics of large riverine reservoirs are still not fully understood because of the complicated hydrodynamics generated by dam operation. We examined how integrated hydrodynamics drive phytoplankton blooms in the XXB, a tributary bay in the TGR, China. The results showed hydrodynamic processes control blooms rather than changes in the abiotic factors like temperature and nutrients, which were sufficient for growth year-round. In the colder months from October to February when the mixed layer is deep, vertical mixing is the dominant hydrodynamic process that prevents blooms from forming. However, during the warmer months from May to July with intense stratification, horizontal advection is more important, and under circulation patterns with stronger surface flows, can suppress blooms by dilution and flushing. This highlights the significance of flushing and dilution in the development and collapse of summer blooms and, extends the application of critical turbulence model when explaining bloom dynamics in dynamic riverine systems like XXB. Instead of the Three Gorges Dam regulation measures like enlarging daily water level fluctuation, which affects dam security and economic benefits, we propose a potential approach to control phytoplankton blooms: withdrawing the warm surface water from upstream cascade reservoirs might increase flows in the surface layer of the tributary bay so as to shift the circulation patterns and reduce summer blooms. We therefore offered perspectives for future studies to investigate the effectiveness of this potential withdrawal strategy.

**Acknowledgements**

This research is supported by the National Key R&D Program of China (2016YFE0133700), the National Natural Science Foundation of China (U2243238, 12002332), the China Scholarship Council (CSC), and the Helmholtz-Centre for Environmental Research (UFZ) program integration budget. We are grateful to the funding institutions for their support. We also thank the editor and three anonymous reviewers who provided constructive comments and suggestions to improve the manuscript.

**References**

Amour, I. and Kauranne, T., 2017. A variational ensemble Kalman filtering method for data assimilation using 2D and 3D version of COHERENS model. International Journal for Numerical Methods in Fluids 83(6), 544-558.

Andreas, Holbach, Lijing, Wang, Stefan and Norra, 2014. Three Gorges Reservoir: Density Pump Amplification of Pollutant Transport into Tributaries. Environmental Science & Technology Es & T.

Bocaniov, S.A., Ullmann, C., Rinke, K., Lamb, K.G. and Boehrer, B., 2014. Internal waves and mixing in a stratified reservoir: Insights from three-dimensional modeling. Limnologica 49, 52-67. https://dx.doi.org/10.1016/j.limno.2014.08.004.

Bowie, G.L., Mills, W.B., Porcella, D.B., Campbell, C.L. and Gherini, S.A., 1985. Rates, constants, and kinetics formulations, Surface Water Quality Modeling.

Burford, M.A., Johnson, S.A., Cook, A.J., Packer, T.V., Taylor, B.M. and Townsley, E.R., 2007. Correlations between watershed and reservoir characteristics, and algal blooms in subtropical reservoirs. Water Research 41(18), 4105-4114. https://dx.doi.org/https://doi.org/10.1016/j.watres.2007.05.053.

Carraro, E., Guyennon, N., Hamilton, D., Valsecchi, L., Manfredi, E.C., Viviano, G., Salerno, F., Tartari, G. and Copetti, D., 2012. Coupling high-resolution measurements to a three-dimensional lake model to assess the spatial and temporal dynamics of the cyanobacterium Planktothrix rubescens in a medium-sized lake. Hydrobiologia 698(1), 77-95. https://dx.doi.org/10.1007/s10750-012-1096-y.

Cerco, C.F., 1993. Three-dimensional eutrophication model of Chesapeake Bay. Journal of Environmental Engineering 119(119), 1006-1025.

Chuo, M., Ma, J., Liu, D. and Yang, Z., 2019. Effects of the impounding process during the flood season on algal blooms in Xiangxi Bay in the Three Gorges Reservoir, China. Ecological Modelling 392, 236-249. https://dx.doi.org/10.1016/j.ecolmodel.2018.11.017.

Dai, H., Mao, J., Jiang, D. and Wang, L., 2013. Longitudinal hydrodynamic characteristics in reservoir tributary embayments and effects on algal blooms. PLoS One 8(7), e68186. https://dx.doi.org/10.1371/journal.pone.0068186.

de Boyer Montégut, C., 2004. Mixed layer depth over the global ocean: An examination of profile data and a profile-based climatology. Journal of Geophysical Research 109(C12). https://dx.doi.org/10.1029/2004jc002378.

Deltares, 2013. Delft3D-FLOW user mannual. The Netherlands, Delft Hydraulics.

Dutta, R.K. and Das, B., 2020. Modeling curtain weirs for controlling algal blooms in the largest tributary of the Three Gorges Reservoir, China. Alexandria Engineering Journal 59(1), 323-332.

https://dx.doi.org/10.1016/j.aej.2019.12.044.

Ezer, T. and Mellor, G.L., 2004. A generalized coordinate ocean model and a comparison of the bottom boundary layer dynamics in terrain-following and in z-level grids. Ocean Modelling 6(3-4), 379-403. https://dx.doi.org/10.1016/s1463-5003(03)00026-x.

Fenocchi, A., Rogora, M., Morabito, G., Marchetto, A., Sibilla, S. and Dresti, C., 2019. Applicability of a one-dimensional coupled ecological-hydrodynamic numerical model to future projections in a very deep large lake (Lake Maggiore, Northern Italy/Southern Switzerland). Ecological Modelling 392, 38-51. https://dx.doi.org/10.1016/j.ecolmodel.2018.11.005.

Fu, B.J., Wu, B.F., Lu, Y.H., Xu, Z. and Zhou, Y.M., 2010. Three Gorges Project: Efforts and challenges for the environment. Progress in Physical Geography 34(6), 741-754.

Gao, Q., He, G., Fang, H., Bai, S. and Huang, L., 2018. Numerical simulation of water age and its potential effects on the water quality in Xiangxi Bay of Three Gorges Reservoir. Journal of Hydrology.

Hai, Hans W. Paerl, Boqiang Qin, Guangwei Zhu and Gao, G., 2010. Nitrogen and phosphorus inputs control phytoplankton growth in eutrophic Lake Taihu, China. Limnology and Oceanography 55(1), 420-432.

He, W., Feng, S., Bi, Y., Jiang, A., Li, Y., Huang, W., Zhang, J., Xu, H. and Liu, C., 2023. Influences of water level fluctuation on water exchange and nutrient distribution in a bay: Evidence from the Xiangxi Bay, Three Gorges Reservoir. Environ Res 222, 115341. https://dx.doi.org/10.1016/j.envres.2023.115341.

Hedger, R., Olsen, N., George, D., Malthus, T. and Atkinson, P., 2004. Modelling spatial distributions of Ceratium hirundnella and Microcystis. in a small productive British lake. Hydrobiologia 528(1-3), 217-227.

Holbach, A., Norra, S., Wang, L., Yuan, Y., Hu, W., Zheng, B. and Bi, Y., 2014. Three Gorges Reservoir: density pump amplification of pollutant transport into tributaries. Environ Sci Technol 48(14), 7798-7806. https://dx.doi.org/10.1021/es501132k.

Huang, T., Wen, C., Wang, S., Wen, G., Li, K., Zhang, H. and Wang, Z., 2022. Controlling spring Dinoflagellate blooms in a stratified drinking water reservoir via artificial mixing: Effects, mechanisms, and operational thresholds. Science of The Total Environment 847. https://dx.doi.org/10.1016/j.scitotenv.2022.157400.

Huisman, J., Codd, G.A., Paerl, H.W., Ibelings, B.W., Verspagen, J.M.H. and Visser, P.M., 2018. Cyanobacterial blooms. Nat Rev Microbiol 16(8), 471-483. https://dx.doi.org/10.1038/s41579-018-0040-1.

Huisman, J., Oostveen, P.V. and Weissing, F.J., 1999. Critical depth and critical turbulence: Two

different mechanisms for the development of phytoplankton blooms. Limnology & Oceanography 44(7).

Ishikawa, M., Gurski, L., Bleninger, T., Rohr, H., Wolf, N. and Lorke, A., 2022. Hydrodynamic Drivers of Nutrient and Phytoplankton Dynamics in a Subtropical Reservoir. Water 14(10). https://dx.doi.org/10.3390/w14101544.

Janssen, A.B.G., Janse, J.H., Beusen, A.H.W., Chang, M., Harrison, J.A., Huttunen, I., Kong, X., Rost, J., Teurlincx, S., Troost, T.A., van Wijk, D. and Mooij, W.M., 2019. How to model algal blooms in any lake on earth. Current Opinion in Environmental Sustainability 36, 1-10. https://dx.doi.org/10.1016/j.cosust.2018.09.001.

Ji, D.B., Wells, S.A., Yang, Z.J., Liu, D.F., Huang, Y.L., Ma, J. and Berger, C.J., 2017. Impacts of water level rise on algal bloom prevention in the tributary of Three Gorges Reservoir, China. Ecological Engineering 98, 70-81. https://dx.doi.org/10.1016/j.ecoleng.2016.10.019.

Jöhnk, K.D., Huisman, J., Sharples, J., Sommeijer, B., Visser, P.M. and Stroom, J.M., 2008. Summer heatwaves promote blooms of harmful cyanobacteria. Blackwell Publishing Ltd 14(3), 495-512.

Köhler, J., Wang, L., Guislain, A. and Shatwell, T., 2018. Influence of vertical mixing on light-dependency of phytoplankton growth. Limnology and Oceanography 63(3), 1156-1167. https://dx.doi.org/10.1002/lno.10761.

Li, J., Jin, Z. and Yang, W., 2014. Numerical modeling of the Xiangxi River algal bloom and sediment-related process in China. Ecological Informatics 22(Supplement C), 23-35. https://dx.doi.org/https://doi.org/10.1016/j.ecoinf.2014.03.002.

Li, J., Yang, W., Li, W., Mu, L. and Jin, Z., 2018. Coupled hydrodynamic and water quality simulation of algal bloom in the Three Gorges Reservoir, China. Ecological Engineering 119, 97-108. https://dx.doi.org/10.1016/j.ecoleng.2018.05.018.

Li, P., Yao, Y., Lian, J. and Ma, C., 2021. Effect of thermal stratified flow on algal blooms in a tributary bay of the Three Gorges Reservoir. Journal of Hydrology. https://dx.doi.org/10.1016/j.jhydrol.2021.126648.

Li, Y., Sun, J., Lin, B. and Liu, Z., 2020. Thermal-hydrodynamic circulations and water fluxes in a tributary bay of the Three Gorges Reservoir. Journal of Hydrology 585. https://dx.doi.org/10.1016/j.jhydrol.2019.124319.

Lian, J., Yao, Y., Ma, C. and Guo, Q., 2014. Reservoir Operation Rules for Controlling Algal Blooms in a Tributary to the Impoundment of Three Gorges Dam. Water 6(10), 3200.

Liu, B. and de Swart, H.E., 2015. Impact of river discharge on phytoplankton bloom dynamics in eutrophic estuaries: A model study. Journal of Marine Systems 152, 64-74. https://dx.doi.org/10.1016/j.jmarsys.2015.07.007.

Liu, B., de Swart, H.E. and de Jonge, V.N., 2018. Phytoplankton bloom dynamics in turbid, well-mixed estuaries: A model study. Estuarine, Coastal and Shelf Science 211, 137-151. https://dx.doi.org/10.1016/j.ecss.2018.01.010.

Liu, D., Huang, Y. and Ji, D., 2013. Algal blooms and ecological regulation in tributaries of Three Gorges Reservoir China Water Resources and Hydropower Press.

Liu, L., Liu, D., Johnson, D.M., Yi, Z. and Huang, Y., 2012. Effects of vertical mixing on phytoplankton blooms in Xiangxi Bay of Three Gorges Reservoir: Implications for management. Water Research 46(7), 2121-2130. https://dx.doi.org/10.1016/j.watres.2012.01.029.

Long, L., Chen, P., Xu, H., Ji, D., Liu, L., Yang, Z. and Lorke, A., 2022. Recent changes of the thermal structure in Three Gorges Reservoir, China and its impact on algal bloom in tributary bays. Ecological Indicators 144, 109465. https://dx.doi.org/https://doi.org/10.1016/j.ecolind.2022.109465.

Long, L.H., Ji, D.B., Yang, Z.J., Ma, J., Wells, S.A., Liu, D.F. and Lorke, A., 2019. Density-driven water circulation in a typical tributary of the Three Gorges Reservoir, China. River Research and Applications 35(7), 833-843. https://dx.doi.org/10.1002/rra.3459.

Lucas, L.V., Thompson, J.K. and Brown, L.R., 2009. Why are diverse relationships observed between phytoplankton biomass and transport time? Limnology and Oceanography 54(1), 381-390. https://dx.doi.org/10.4319/lo.2009.54.1.0381.

Mao, J., Jiang, D. and Dai, H., 2015. Spatial–temporal hydrodynamic and algal bloom modelling analysis of a reservoir tributary embayment. Journal of Hydro-environment Research 9(2), 200-215. https://dx.doi.org/https://doi.org/10.1016/j.jher.2014.09.005.

Marcé, R., FeijoÓ, C., Navarro, E., OrdoÑEz, J., GomÀ, J. and Armengol, J., 2007. Interaction between wind-induced seiches and convective cooling governs algal distribution in a canyon-shaped reservoir. Freshwater Biology 52(7), 1336-1352. https://dx.doi.org/10.1111/j.1365-2427.2007.01771.x.

Marshall, H.G. and Burchardt, L., 1998. Phytoplankton Composition Within The Tidal Freshwater Region Of The James River, Virginia. Proceedings of the Biological Society of Washington (111), 720-730.

Mcgregor, G.B. and Fabbro, L.D., 2000. Dominance of Cylindrospermopsis raciborskii (Nostocales, Cyanoprokaryota) in Queensland tropical and subtropical reservoirs: Implications for monitoring and management. Lakes & Reservoirs: Research & Management 5(3), 195-205.

Mi, C., Hamilton, D.P., Frassl, M.A., Shatwell, T., Kong, X., Boehrer, B., Li, Y., Donner, J. and Rinke, K., 2022. Controlling blooms of Planktothrix rubescens by optimized metalimnetic water withdrawal: a modelling study on adaptive reservoir operation. Environmental Sciences Europe 34(1). https://dx.doi.org/10.1186/s12302-022-00683-3.

Mi, C., Rinke, K. and Shatwell, T., 2023. Optimizing selective withdrawal strategies to mitigate hypoxia under water-level reduction in Germany's largest drinking water reservoir. Journal of Environmental Sciences. https://dx.doi.org/https://doi.org/10.1016/j.jes.2023.06.025.

Mi, C., Shatwell, T., Ma, J., Wentzky, V.C., Boehrer, B., Xu, Y. and Rinke, K., 2020. The formation of a metalimnetic oxygen minimum exemplifies how ecosystem dynamics shape biogeochemical processes: A modelling study. Water Res 175, 115701. https://dx.doi.org/10.1016/j.watres.2020.115701.

Ministry of Environmental Protection of China, L., 2014. Bulletin on the ecological and environmental monitoring results of the TGP (2003-2013).

Mitrovic, S.M., Oliver, R.L., Rees, C., Bowling, L.C. and Buckney, R.T., 2010. Critical flow velocities for the growth and dominance of Anabaena circinalis in some turbid freshwater rivers. Freshwater Biology 48.

Molen, D., Los, F.J., Ballegooijen, L.V. and Vat, M.D., 1994. Mathematical modelling as a tool for management in eutrophication control of shallow lakes. Hydrobiologia 275-276(1), 479-492.

Nicklisch, A., Shatwell, T. and Kohler, J., 2008. Analysis and modelling of the interactive effects of temperature and light on phytoplankton growth and relevance for the spring bloom. Journal of Plankton Research 30(1), 75-91. https://dx.doi.org/10.1093/plankt/fbm099.

Paerl, H.W. and Huisman, J., 2008. Blooms Like It Hot. Science 320(5872), p.57-58.

Paerl, H.W. and Huisman, J., 2010. Climate change: a catalyst for global expansion of harmful cyanobacterial blooms. Environmental Microbiology Reports 1(1).

Paerl, H.W., Xu, H., McCarthy, M.J., Zhu, G., Qin, B., Li, Y. and Gardner, W.S., 2011. Controlling harmful cyanobacterial blooms in a hyper-eutrophic lake (Lake Taihu, China): the need for a dual nutrient (N & P) management strategy. Water Res 45(5), 1973-1983. https://dx.doi.org/10.1016/j.watres.2010.09.018.

Qin, Z., 1980. A contribution to the calculation of wind stress on sea surface. Trans Oceanology Limn 3, 1-8.

Reynolds, C.S., 2000. Hydroecology of river plankton: the role of variability in channel flow. Hydrological Processes 14(16-17), 3119-3132. https://dx.doi.org/10.1002/1099-1085(200011/12)14:16/17<3119::Aid-hyp137>3.0.Co;2-6.

Robson, B.J., Hamilton, D.P., Webster, I.T. and Chan, T., 2013. Ten steps applied to development and evaluation of process-based biogeochemical models of estuaries. Environmental Modelling and Software 23(4), 369-384.

Scheffer and Van, 2007. Shallow lakes theory revisited: various alternative regimes driven by climate, nutrients, depth and lake size. Shallow Lakes Changing World 2007 196, 455-466.

Schindler, D.W., Carpenter, S.R., Chapra, S.C., Hecky, R.E. and Orihel, D.M., 2016. Reducing Phosphorus to Curb Lake Eutrophication is a Success. Environmental Science & Technology 50(17), 8923.

Sha, Y., Wei, Y., Li, W., Fan, J. and Cheng, G., 2015. Artificial tide generation and its effects on the water environment in the backwater of Three Gorges Reservoir. Journal of Hydrology 528, 230-237.

Shatwell, T., Nicklisch, A. and Köhler, J., 2012. Temperature and photoperiod effects on phytoplankton growing under simulated mixed layer light fluctuations. Limnology and Oceanography 57(2), 541-553. https://dx.doi.org/10.4319/lo.2012.57.2.0541.

Soballe, D.M. and Kimmel, B.L., 1987. A Large‐Scale Comparison of Factors Influencing Phytoplankton Abundance in Rivers, Lakes, and Impoundments. Ecology A Publication of the Ecological Society of America 68(6), 1943-1954.

Sommer, U., Gliwicz, Z.M., Lampert, W.I. and Duncan, A., 1986. The PEG-model of seasonal succession of planktonic events in fresh waters. Archiv fur Hydrobiologie 106(4), 433-471.

Song, Y., 2023. Hydrodynamic impacts on algal blooms in reservoirs and bloom mitigation using reservoir operation strategies: A review. Journal of Hydrology 620. https://dx.doi.org/10.1016/j.jhydrol.2023.129375.

Song, Y., Chen, M., Li, J., Zhang, L., Deng, Y. and Chen, J., 2023. Can selective withdrawal control algal blooms in reservoirs? The underlying hydrodynamic mechanism. Journal of Cleaner Production 394, 136358. https://dx.doi.org/https://doi.org/10.1016/j.jclepro.2023.136358.

Song, Y., Shen, L., Zhang, L., Li, J. and Chen, M., 2021. Study of a hydrodynamic threshold system for controlling dinoflagellate blooms in reservoirs. Environ Pollut 278, 116822. https://dx.doi.org/10.1016/j.envpol.2021.116822.

Song, Y., You, L., Chen, M., Li, J., Zhang, L. and Peng, T., 2022. Key hydrodynamic principles for controlling algal blooms using emergency reservoir operation strategies. J Environ Manage 325(Pt A), 116470. https://dx.doi.org/10.1016/j.jenvman.2022.116470.

Sun, J., Zhou, J., Zhang, M. and Lin, B., 2019. Investigation on hydrothermal processes in a large channel-type reservoir using an integrated physics-based model. Journal of Hydroinformatics 21(3), 493-509. https://dx.doi.org/10.2166/hydro.2019.139.

Sverdrup, 1953. On conditions for the vernal blooming of phytoplanktopn. ICES Journal of Marine Science 18(3), 287-295.

Visser, P.M., Ibelings, B.W., Bormans, M. and Huisman, J., 2015. Artificial mixing to control cyanobacterial blooms: a review. Aquatic Ecology 50(3), 423-441. https://dx.doi.org/10.1007/s10452-015-9537-0.

Visser, P.M., Verspagen, J.M.H., Sandrini, G., Stal, L.J., Matthijs, H.C.P., Davis, T.W., Paerl, H.W.

and Huisman, J., 2016. How rising CO2 and global warming may stimulate harmful cyanobacterial blooms. Harmful Algae 54(apr.), 145-159.

Wilson, H.L., Ayala, A.I., Jones, I.D., Rolston, A., Pierson, D., de Eyto, E., Grossart, H.-P., Perga, M.-E., Woolway, R.I. and Jennings, E., 2020. Variability in epilimnion depth estimations in lakes. Hydrology and Earth System Sciences. https://dx.doi.org/10.5194/hess-2020-222.

Wurtsbaugh, W.A., Paerl, H.W. and Dodds, W.K., 2019. Nutrients, eutrophication and harmful algal blooms along the freshwater to marine continuum. Wiley Interdisciplinary Reviews: Water 6(5), e1373.

Xiang, R., Wang, L., Li, H., Tian, Z. and Zheng, B., 2021. Water quality variation in tributaries of the Three Gorges Reservoir from 2000 to 2015. Water Res 195, 116993. https://dx.doi.org/10.1016/j.watres.2021.116993.

Xu, H., Yan, M., Long, L., Ma, J., Ji, D., Liu, D. and Yang, Z., 2021. Modeling the Effects of Hydrodynamics on Thermal Stratification and Algal Blooms in the Xiangxi Bay of Three Gorges Reservoir. Frontiers in Ecology and Evolution 8. https://dx.doi.org/10.3389/fevo.2020.610622.

Yang, L., Liu, D., Huang, Y., Yang, Z., Ji, D. and Song, L., 2015. Isotope analysis of the nutrient supply in Xiangxi Bay of the Three Gorges Reservoir. Ecological Engineering 77, 65-73. https://dx.doi.org/10.1016/j.ecoleng.2015.01.013.

Yang, Z., Cheng, B., Xu, Y., Liu, D., Ma, J. and Ji, D., 2018a. Stable isotopes in water indicate sources of nutrients that drive algal blooms in the tributary bay of a subtropical reservoir. Sci Total Environ 634, 205-213. https://dx.doi.org/10.1016/j.scitotenv.2018.03.266.

Yang, Z., Liu, D., Ji, D., Xiao, S., Huang, Y. and Ma, J., 2013. An eco-environmental friendly operation: An effective method to mitigate the harmful blooms in the tributary bays of Three Gorges Reservoir. Science China Technological Sciences 56(6), 1458-1470. https://dx.doi.org/10.1007/s11431-013-5190-9.

Yang, Z., Wei, C., Liu, D., Lin, Q., Huang, Y., Wang, C., Ji, D., Ma, J. and Yang, H., 2022. The influence of hydraulic characteristics on algal bloom in Three Gorges Reservoir, China: A combination of cultural experiments and field monitoring. Water Research. https://dx.doi.org/10.1016/j.watres.2021.118030.

Yang, Z., Xu, P., Liu, D., Ma, J., Ji, D. and Cui, Y., 2018b. Hydrodynamic mechanisms underlying periodic algal blooms in the tributary bay of a subtropical reservoir. Ecological Engineering 120, 6-13. https://dx.doi.org/10.1016/j.ecoleng.2018.05.003.

Zhang, F., Li, M., Glibert, P.M. and Ahn, S.H.S., 2021. A three-dimensional mechanistic model of Prorocentrum minimum blooms in eutrophic Chesapeake Bay. Science of The Total Environment 769, 144528.

Zhang, F., Zhang, H., Bertone, E., Stewart, R., Lemckert, C. and Cinque, K., 2020. Numerical study of the thermal structure of a stratified temperate monomictic drinking water reservoir. Journal of Hydrology: Regional Studies 30. https://dx.doi.org/10.1016/j.ejrh.2020.100699.

Zhang, Y., Liu, D.F., Ji, D.B., Yang, Z.J. and Chen, Y.Y., 2012. Effects of intrusions from Three Gorges Reservoir on nutrient supply to Xiangxi Bay. Environmental Science (in Chinese) 33(8), 2621-2627.

Zhou, 2006. Discussion on Three Gorges Powerplant to Modulate More Net-peaks to Improve Water Quality of Tributaries of Reservoir. Science & Technology Review 23(0510), 8-12.

## Figures

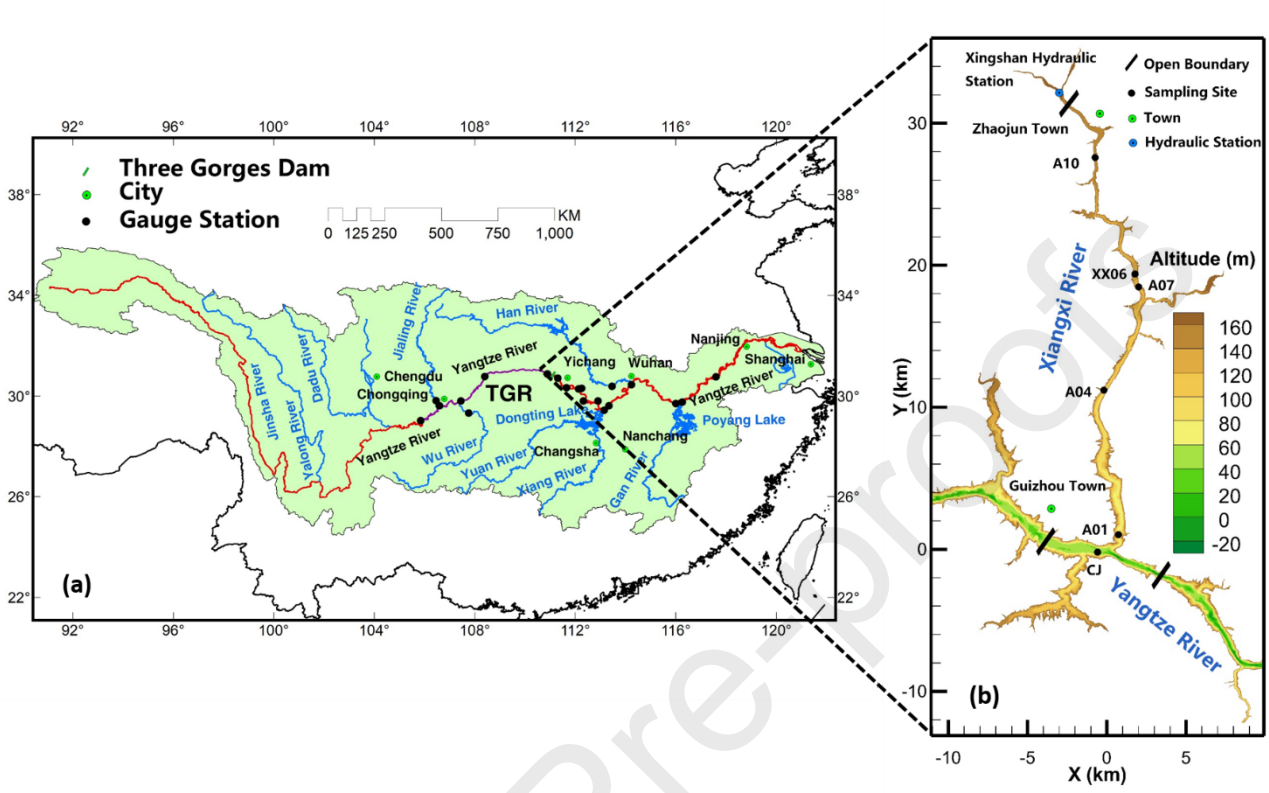


Fig. 1. Geography of the TGR and XXB. (a) The Yangtze basin, with the locations of the Three Gorges Dam and TGR, the red line represents the main stream of the Yangtze and the purple line represents the area of the TGR. (b) The study area of model, with elevation of the XXB bottom, and sampling sites in the XXB.

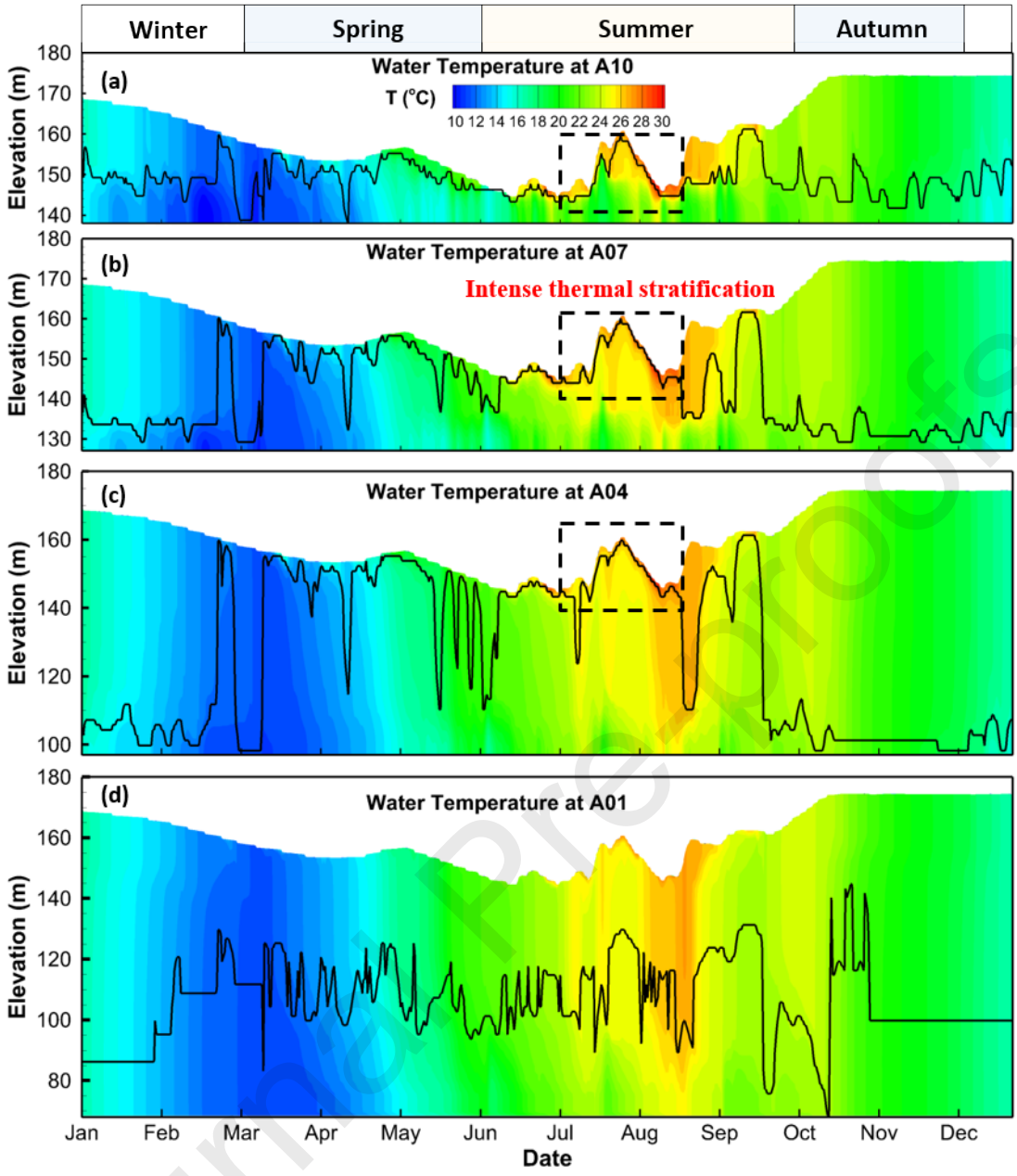


Fig. 2. Distribution of laterally averaged water temperature and mixed layer depth (black line) in A10 (a), A07 (b), A04 (c), and A01 (d), respectively in 2010.

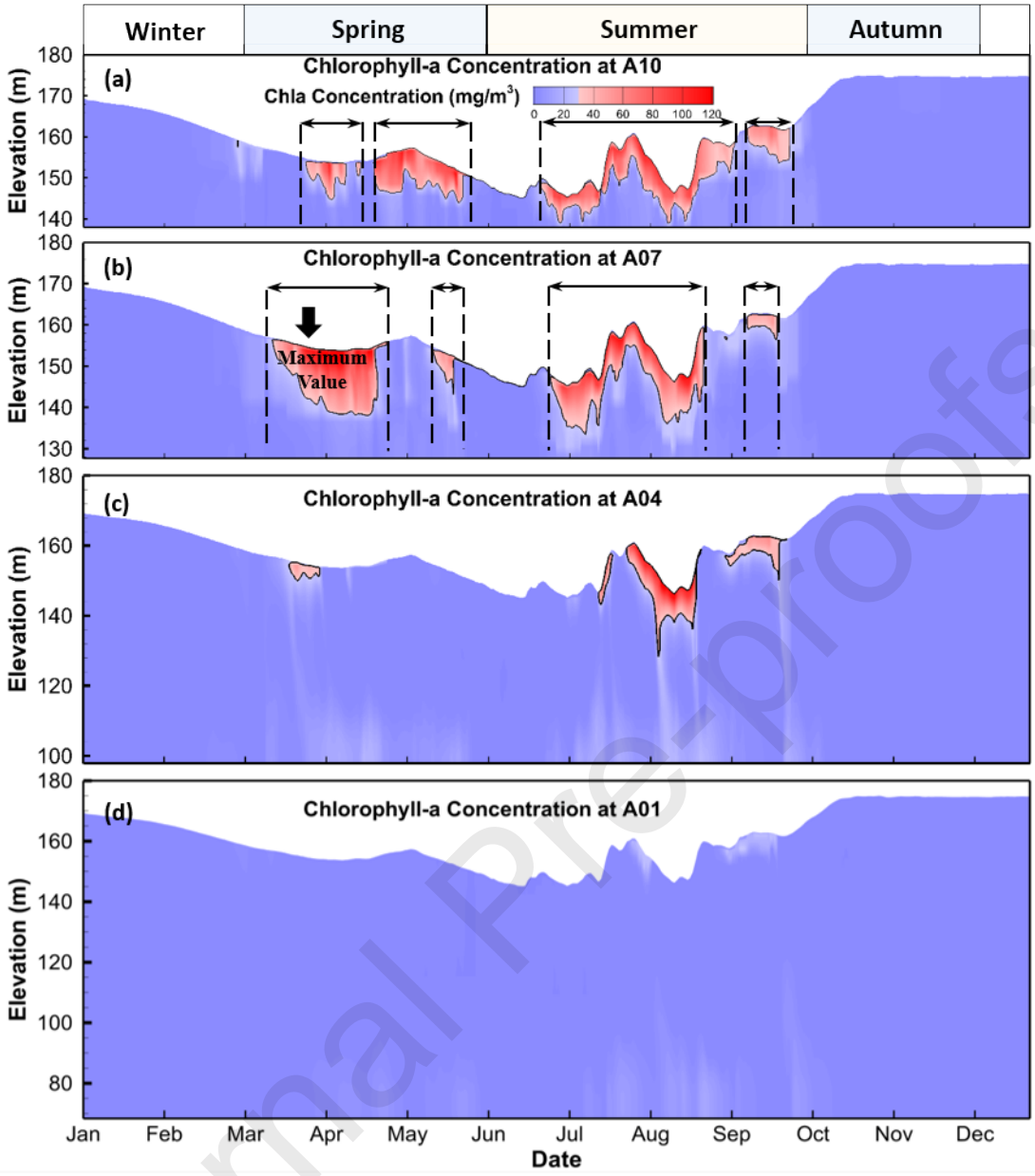

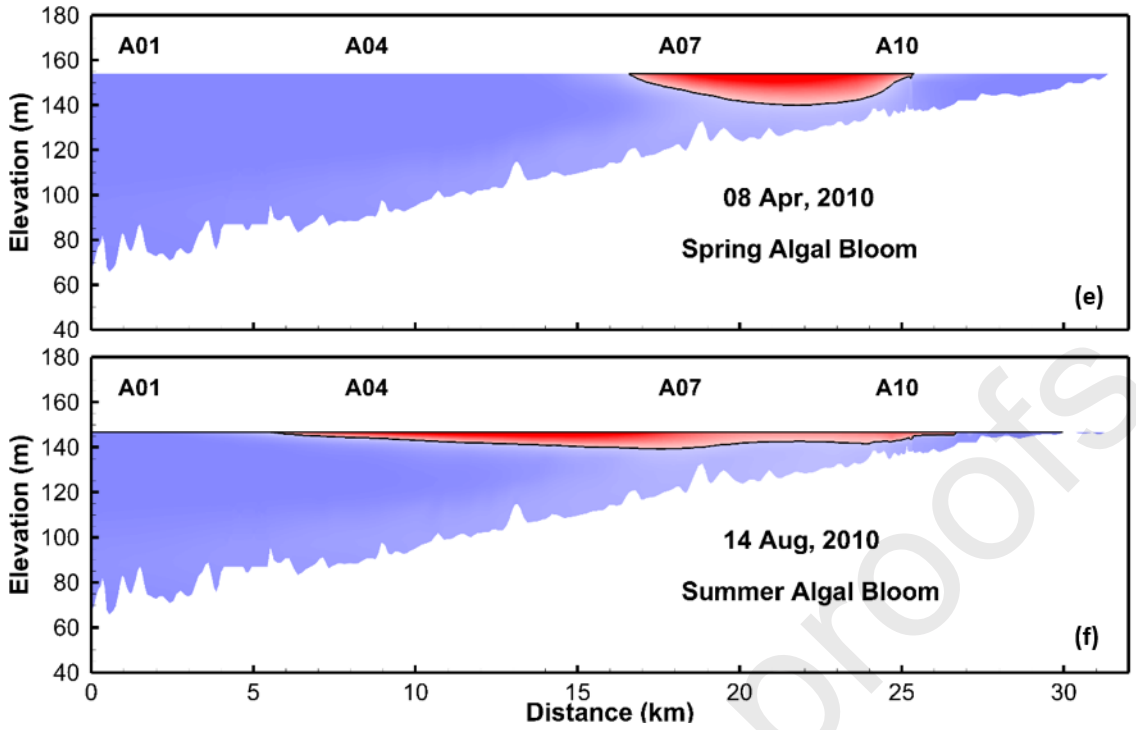


**Fig. 3.** Seasonal distribution of Chl-a concentration in A10 (a), A07 (b), A04 (c), and A01 (d); and spatial distribution of Chl-a concentration along the thalweg during the spring phytoplankton bloom (e) and the summer phytoplankton bloom (f). Red colour represents a Chl-a concentration over 30 mg $m^{-3}$, our threshold for phytoplankton blooms, and blue represents Chl-a concentration below 30 mg $m^{-3}$.

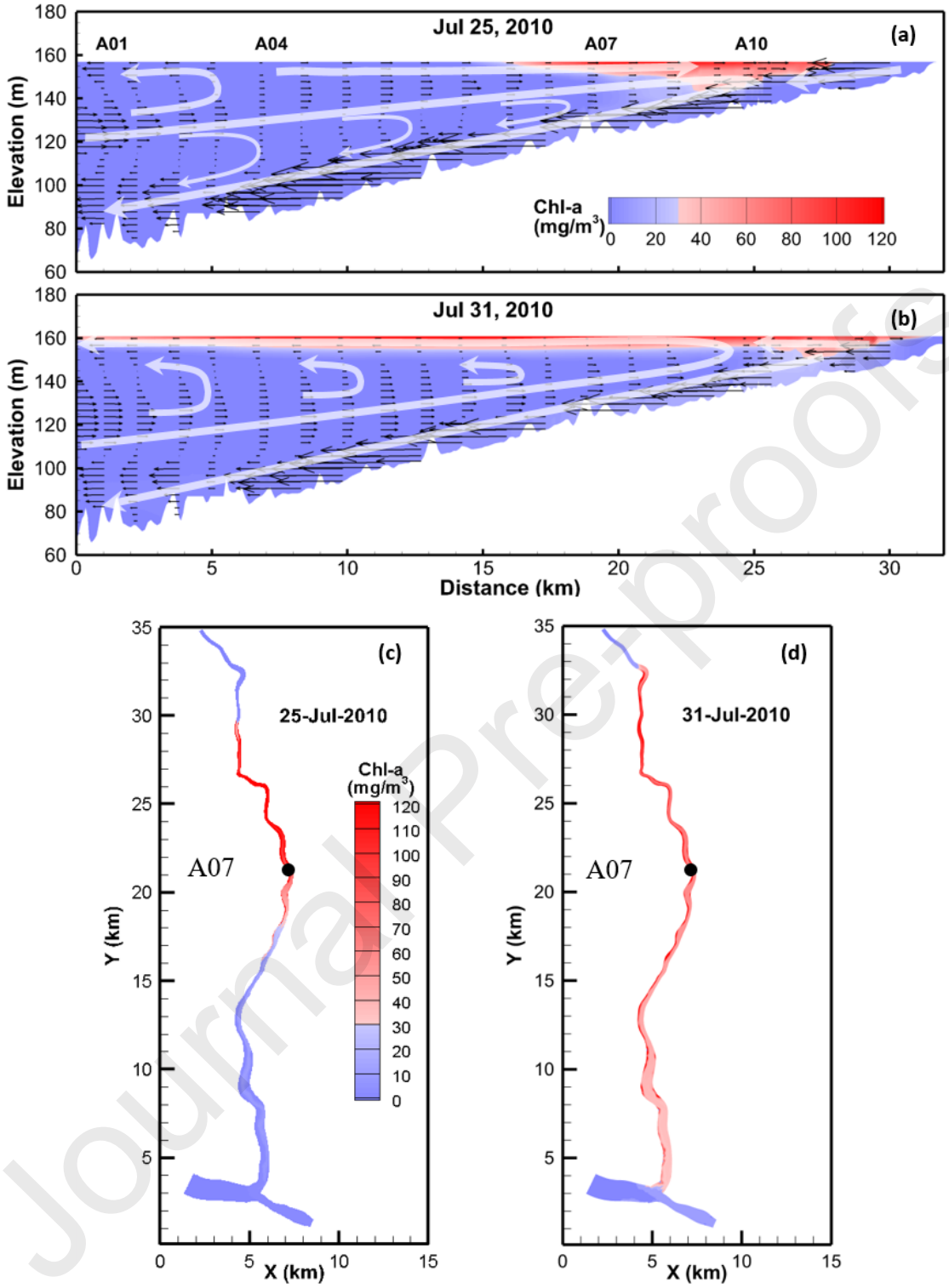


Fig. 4. The Chl-a concentration distribution and circulation patterns along the central line during a phytoplankton bloom collapse period (a) on Jul 25 (b) on Jul 31 and the horizontal distribution of surface Chl-a concentration (c) on Jul 25 (d) on Jul 31. The white arrows indicate the circulation patterns.

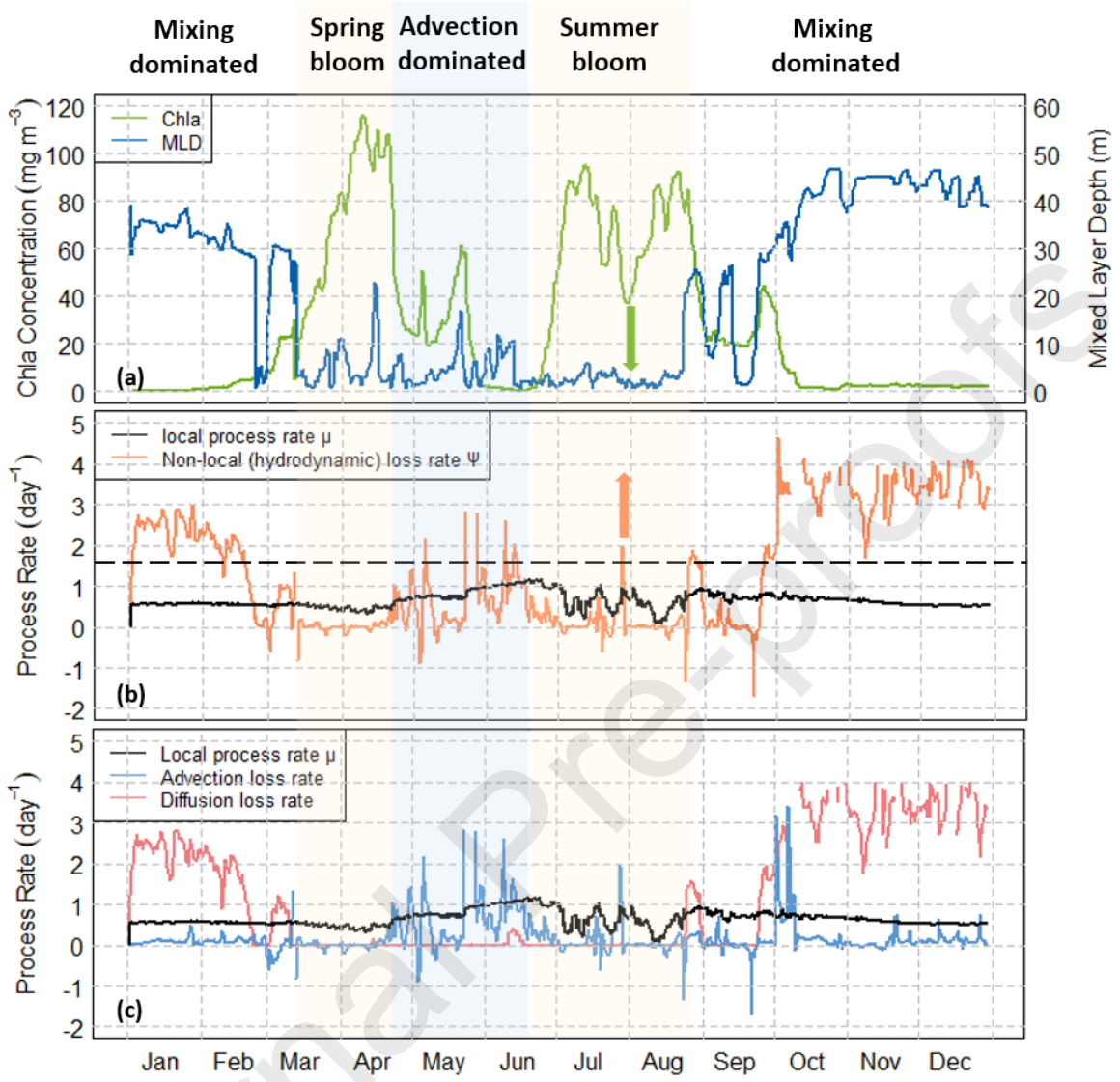


**Fig. 5.** (a) Surface Chl-a concentration (green line) and mixed layer depth (dark blue line) at middle reach of XXB (Station A07). (b) Process rate to the phytoplankton growth and collapse. The black line indicates the local (specific net growth of phytoplankton) process rate $\mu$, the orange line indicates the non-local (hydrodynamic) loss rate $\psi$ to phytoplankton growth (see Eq. 5). (c) shows the same processes as (b) where the black line indicates $\mu$, but $\psi$ have been resolved into the horizontal advection component (light blue line) and vertical diffusion component (red line), for $\psi$, vertical diffusion loss rate and horizontal advection loss rate, the positive value indicates the loss processes and the negative value indicates the growth processes. The orange arrow indicates an increase in the $\psi$ and the green arrow indicates a decrease of the Chl-a concentration correspondingly. The black dashed line indicates the maximum specific growth rate $\mu_{max}$ of phytoplankton. The yellow shade regions represent the spring and summer blooms periods, and the blue shade region represents advection dominated periods during the warm months when blooms were suppressed by dilution and flushing.

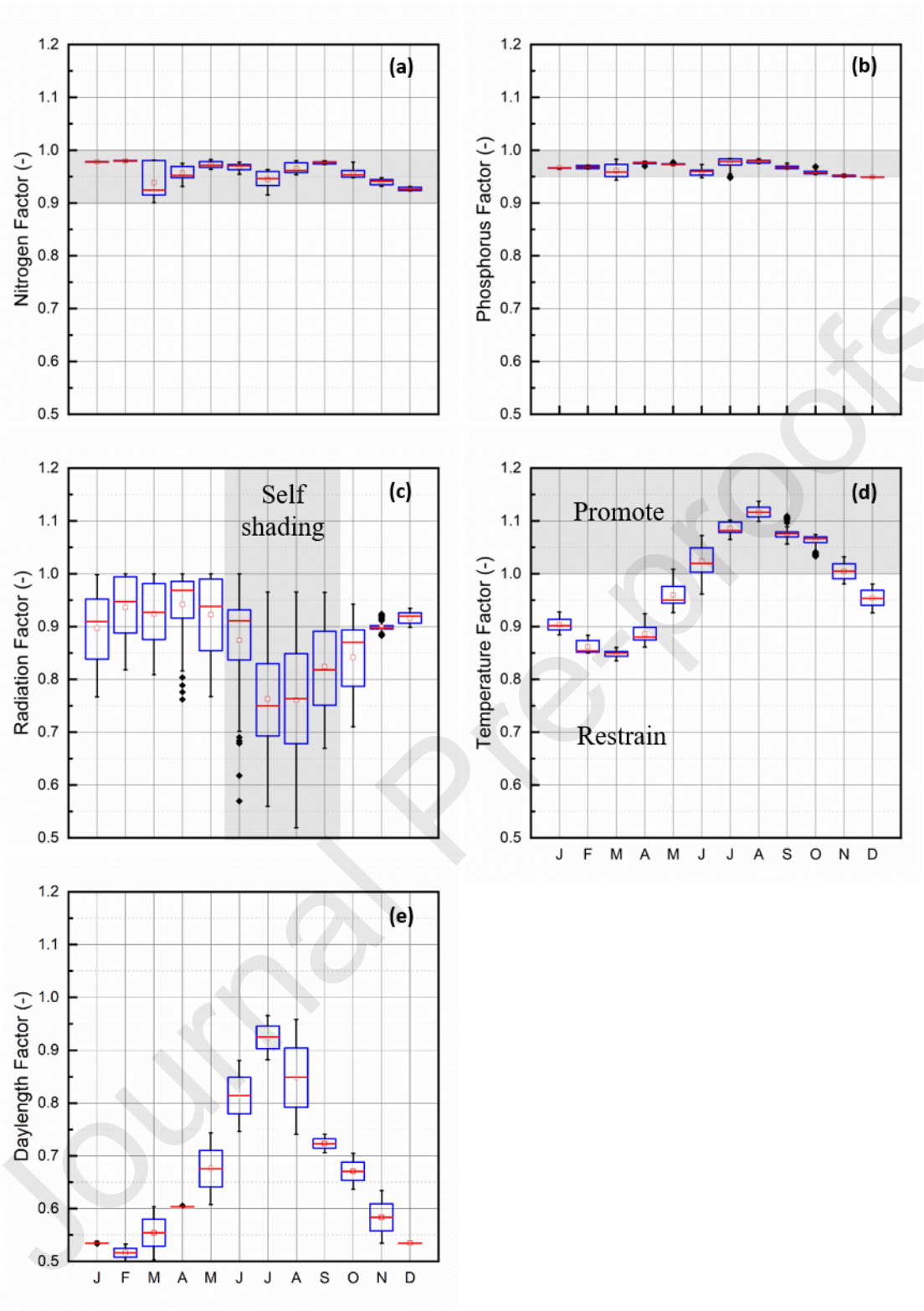


**Fig. 6.** Environmental limitation factor of local (specific net growth of phytoplankton) processes $\mu$ at station A07 in the surface layer, (a) nitrogen limitation factor ($g_1$ ($n$) in Eq. (S5)), (b) phosphorus limitation factor ($g_2$ ($p$) in Eq. (S6)), (c) radiation limitation factor ($h_1$ ($I$) in Eq. (S2)), (d) temperature limitation factor ($f_3$ ($T$) in Eq. (S7)), and (e) daylength limitation factor ($h_2$ ($DL$) in Eq. (S3)). Red lines denote medians of the limitation factors, blue rectangles denote the first and third quartiles, the whiskers represent the maximum and minimum value, and black points denote the outliers.

## Tables

**Table 1.** Main water quality parameter list for the XXB.

| Parameters | Description | Unit | Value used |
|---|---|---|---|
| *PPMax* | Maximum growth rate of phytoplankton at 20 °C | $day^{-1}$ | 1.8[a] |
| *Mort* | Mortality rate of phytoplankton at 20 °C | $day^{-1}$ | 0.08[a, b] |
| *MResp* | Respiration rate of phytoplankton at 20 °C | $day^{-1}$ | 0.1[a] |
| *KKmDIN* | Phytoplankton half saturation constant for uptake N | $mg\ L^{-1}$ | 0.025[a] |
| *KmP* | Phytoplankton half saturation constant for uptake P | $mg\ L^{-1}$ | 0.005[a] |
| *ku_dFdcC* | Mineralization rate of detritus C | $day^{-1}$ | 0.15[a] |
| *ku_dFdcP* | Mineralization rate of detritus P | $day^{-1}$ | 0.15[a] |
| *ku_dFdcN* | Mineralization rate of detritus N | $day^{-1}$ | 0.12[a] |
| *RcNit* | Nitrification rate constant | $day^{-1}$ | 0.1[d, e] |
| *RcDen* | Denitrification rate constant | $day^{-1}$ | 0.1[d, e] |
| *GrToChl* | Chl-a to carbon ratio in phytoplankton | mg Chl-a/g C | 50 [d, e] |
| *PCRat* | P to C ratio in phytoplankton | mg P/mg C | 0.025[a] |
| *NCRat* | N to C ratio in phytoplankton | mg N/mg C | 0.25[a] |
| *VSed* | Settling velocity of phytoplankton | $m\ day^{-1}$ | 0.05[b, c] |
| *TCGro* | The temperature constant for phytoplankton production | - | 1.02[f] |
| *RadSat* | Light saturation intensity of phytoplankton | $W\ m^{-2}$ | 105[f] |

[a] Mao et al., (2015)

[b] Li et al., (2014)

[c] Chuo et al., (2019)

[d] Bowie et al., (1985)

[e] Model defaults values

[f] From calibration

**Highlights**

- 3D ecological-hydrodynamic modelling of Xiangxi Bay for one year
- Diffusion and advection effects on blooms are quantified by scaling criterion
- Algae blooms are inhibited by alternative mechanisms of diffusion/advection
- Application of critical turbulence model was extended to consider advection

**Bo Gai:** Conceptualization, Writing – Original Draft, Writing – Review & Editing, Methodology, Software, Formal analysis, Visualization. **Jian Sun:** Writing – Review & Editing, Resources. **Binliang Lin:** Funding acquisition, Supervision, Writing – Review & Editing. **Yuanyi Li:** Software, Data Curation, Methodology. **Chenxi Mi:** Software, Validation. **Tom Shatwell:** Conceptualization, Writing – Original Draft, Writing – Review & Editing, Supervision, Funding acquisition, Software.